Trace gas detection based on off-beam quartz enhanced photoacoustic spectroscopy: Optimization and performance evaluation

Kun Liu,[1,2] Hongming Yi,[1,2] Anatoliy A. Kosterev,[3] Weidong Chen,[4] Lei Dong,[3] Lei Wang,[1,2] Tu Tan,[1,2] Weijun Zhang,[1,2] Frank K. Tittel,[3] and Xiaoming Gao[1,2,a)]
[1]*Environmental Spectroscopy Laboratory, Anhui Institute of Optics and Fine Mechanics, Chinese Academy of Sciences, Hefei, 230031, People's Republic of China*
[2]*Key Laboratory of Atmospheric Composition and Optical Radiation, Chinese Academy of Sciences, Hefei 230031, China*
[3]*Rice Quantum Institute, MS 366, Rice University, 6100 Main St., Houston, Texas 77005, USA*
[4]*Laboratoire de Physicochimie de l'Atmosphère, CNRS UMR 8101, Université du Littoral Côte d'Opale, 189A, Av. Maurice Schumann, 59140 Dunkerque, France*

(Received 15 April 2010; accepted 27 July 2010; published online 19 October 2010)

A gas sensor based on off-beam quartz enhanced photoacoustic spectroscopy was developed and optimized. Specifically, the length and diameter of the microresonator tube were optimized, and the outer tube shape is modified for enhancing the trace gas detection sensitivity. The impact of the distance between the quartz tuning fork and an acoustic microresonator on the sensor performance was experimentally investigated. The sensor performance was evaluated by determining the detection sensitivity to H_2O vapor in ambient air at normal atmospheric pressure. A normalized noise equivalent absorption coefficient (1σ) of 6.2×10^{-9} cm^{-1} $W/Hz^{1/2}$ was achieved.
 [doi:10.1063/1.3480553]

I. INTRODUCTION

Laser based trace gas sensors have a wide range of potential applications such as environmental monitoring, medical diagnostics, and industrial process control.[1–4] In many cases, highly sensitive, compact, robust, and cost effective trace gas sensors are needed. Such a sensor can be realized using an innovative, sensitive trace gas sensor platform based on photoacoustic spectroscopy (PAS).[5–11] The PAS technique offers several practically important advantages, such as high trace gas detection sensitivity with a small sensing module, wide dynamic range, and no need for an optical detector such as a photodiode. Unlike such spectroscopic techniques as integrated cavity output spectroscopy (ICOS), cavity ring down spectroscopy or absorption spectroscopy in multipass cells, the PAS is a "zero base line" method. In addition, the amplitude of the photoacoustic signal depends on the power of the exciting light beam. Therefore, the PAS can benefit from using continuous wave infrared laser sources capable of emitting high optical power.[12–14] Progress of the PAS technique for trace gas detection has been closely coupled with the development of laser technology. To date, there are several PAS techniques including traditional resonant PAS with wide-band microphones,[6,15] cantilever-based PAS,[16] and quartz enhanced PAS (QEPAS).[17]

QEPAS is a rapidly developing photoacoustic spectroscopy technique for sensitive trace gas detection in a small sample volume, which has been successfully applied to the detection of various simple molecules with narrow absorption spectra[17–23] and larger molecules with broad, unresolved spectral absorption features.[24–26] Several optical excitation sources including near-infrared distributed feedback (DFB) diode lasers,[17–23] midinfrared interband cascade laser,[24] quantum cascade laser,[25,27] and an optical parametric oscillator[28] have been used in the QEPAS technique. The distinguishing feature of QEPAS is the use of a quartz tuning fork (QTF) for detection of the optically generated sound. A QTF is an oscillator with extremely low internal losses; its quality factor Q in vacuum is typically 70 000–110 000. In QEPAS applications, the QTF is immersed in gas, which dampens its motion. Nevertheless, the typical Q of a QTF in air at normal pressure and temperature conditions remains very high, i.e., ~10 000–13 000. The high Q of a QTF is helpful for obtaining an enhanced signal to noise ratio (SNR). Furthermore, the geometry of QTF and the electrical configuration makes it preferentially sensitive to pressure variations in a small volume between its prongs ($\sim0.3\times0.3\times3$ mm^3). Thus, QEPAS detectors have high special selectivity and immunity to environmental acoustic noise. In most of the reported QEPAS works the noise floor was determined by the fundamental thermal noise of the QTF oscillator.[17]

In its simplest implementation, the QEPAS spectrophone consists of only a QTF with a laser beam passing between its prongs.[17,18,29] However, much better sensitivity can be achieved if a rigid metal tube or a pair of tubes [microresonator (mR)] is used to confine and, in some configurations, resonantly amplify the optically generated acoustic signal.[18] In most reported QEPAS sensors, the microresonator consisted of the two tubes symmetrically positioned from both sides of the QTF. An alternative configuration called "off-beam QEPAS" (OB-QEPAS) was first reported in Ref. 30. In OB-QEPAS the laser beam and the QTF are separated by a

a)Tel.: 086-551-5591534. FAX: 086-551-5591560. Electronic mail: xmgao@aiofm.ac.cn.

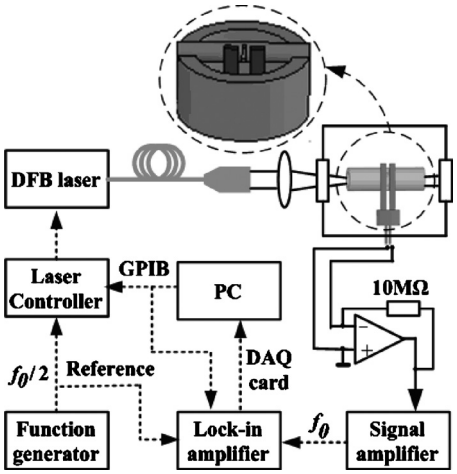

FIG. 1. Schematic of the OB-QEPAS-based gas sensor platform. L: focusing lens with 30 mm focal length and PC: personal computer with data acquisition card and GPIB card. The fiber-coupled DFB diode laser current is modulated at half the QTF resonant frequency f_0.

physical barrier (microresonator walls), QTF sensing the pressure in the microresonator through a small opening in its center. Such a configuration gives certain technical advantages, facilitates the optical alignment, and allows for more flexibility in the QTF dimensions. In this publication we report an in-depth study of the OB-QEPAS spectrophone, its performance and optimum parameters.

In OB-QEPAS, the acoustic oscillations of gas are exited in the mR by a modulated laser source. The photoacoustic signal amplitude in the mR can be written as[2]

$$A = C(\omega)\alpha W, \tag{1}$$

where the quantity $C(\omega)$ is the "cell constant," which describes the characteristics of the mR at a given frequency f, $\omega = 2\pi f$. The modulation frequency of the power input into the gas was set to be the same as the QTF resonant frequency. α is the absorption coefficient of the target gas sample which is related to the gas concentration and absorption cross section. W is the optical power of the laser excitation source.

The acoustic oscillations in the mR give rise to a sound wave radiated via a slit at its center and detected by a QTF placed outside the mR, close to the slit. The piezoelectric current generated by the resonant QTF is proportional to the amplitude of the photoacoustic signal described by Eq. (1) and the Q factor of the QTF. Therefore the OB-QEPAS signal can be written as

$$S = kAQ = kC(\omega)Q\alpha W, \tag{2}$$

where k is a constant describing the transfer characteristics of the QTF. Q is the quality factor of the QTF. With this approach, the mR offers an enhancement factor of ~ 16.[30]

II. OB-QEPAS SENSOR CONFIGURATION

A schematic diagram of the OB-QEPAS based trace gas sensor platform is shown in Fig. 1, and the insert details the positioning of a QTF with respect to the mR. A fiber-coupled DFB diode laser (NLK1E5GAAA, NEL, Yokohama, Japan) tunable from 7154 to 7171 cm^{-1} was used as the excitation light source for generating the photoacoustic signal. This spectral range is suitable for detection of water vapor in air accessing the strong absorption line at 7161.41 cm^{-1} with a line intensity of 1.174×10^{-20} $cm^{-1}/(mol\ cm^{-2})$. The laser current and temperature were controlled by a commercial diode laser controller (ILX Lightwave LDC-3724) (Bozeman, MT). Coarse and fine wavelength tuning was performed by changing the laser temperature and current, respectively. Wavelength modulation and second harmonic detection are used in this work. The laser current was sine wave modulated at half the QTF resonant frequency $f_0/2$ by using a function generator. The laser beam was collimated with a fiber-coupled collimator ($f \sim 4.8$ mm) and subsequently focused into the mR by use of a lens L with a 30 mm focal length. A QTF (DT-38, 32.768–12.5pF, KDS, Daishinku Corp., Kakogawa, Japan) with a resonant frequency of $f_0 = \sim 32.76$ kHz was placed outside the mR for acoustic signal detection. The QTF-generated piezoelectric current was converted into voltage using a custom made transimpedance amplifier with a feedback resistor $R = 10$ MΩ. A signal amplifier (EG&G, Model 5113, AMETEK Advanced Measurement Technology, Wokingham, UK) with a gain of 25 and 6 dB bandpass filter (10–100 kHz) was used for signal filtering and further amplification prior to demodulation at f_0 by a lock-in amplifier (Stanford Research Systems, Model SR 830 DSP). The lock-in amplifier and the laser controller were controlled by a personal computer with a GPIB card and a software program based on LABWINDOWS/CVI. The time constant of the lock-in amplifier was set to 1 s in combination with an 18 dB/octave slope filter ($\Delta f = 0.094$ Hz).

III. SENSOR OPTIMIZATION

The sensor was designed for operation at normal atmospheric pressure. Optimization and performance evaluation of the OB-QEPAS based sensor were carried out in ambient air. Water vapor (H_2O) in air was used as the target species. The H_2O absorption line at 7161.41 cm^{-1} with a line intensity of 1.174×10^{-20} $cm^{-1}/(mol\ cm^{-2})$ was chosen for H_2O detection. The laser wavelength was tuned to this line when its temperature was set to 28 °C at an injection current of 68 mA. The laser power at the target wavelength was measured to be ~8 mW after the fiber collimator lens.

In the OB-QEPAS approach, it is necessary to optimize the mR length, and the optimal length of the mR is dependent on the mR inner diameter. Based on previous experimental investigations, the OB-QEPAS signal increases with decreasing inner diameter of the mR.[30] However, a too small inner diameter makes the optical alignment difficult. Therefore a mR with a 0.5 mm inner diameter and 0.8 mm outer diameter was selected in the present work. The mR was cut out of a syringe needle. The mR slit width was 0.15 ± 0.02 mm with a length of ~0.5 mm, as shown in Fig. 2(a). Initially, the mR was cut to a 13 mm length. Then its length was gradually adjusted by symmetrically cutting off the pieces from both ends. The signal was normalized to the changing H_2O vapor concentration in the ambient air.

Varying the tube length shifts the resonant frequency of

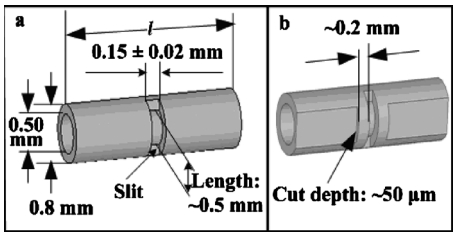

FIG. 2. (a) Dimensions of the microresonator tube. Most experiments were performed with $l=8.0\pm0.1$ mm. (b) Modified mR tube.

the mR, and the QTF works as a fixed-frequency probe. As it was shown in Ref. 31, this is equivalent to exciting and probing the fixed resonator at different frequencies, because the acoustic impedance depends on the product of the resonant and the probe frequencies. In order to find the relation between the tube length and the mR resonance, we can use the theory of finger-holes in woodwind instruments as outlined in Ref. 32. In case of a hole positioned in the center of the tube, the resonant condition from Ref. 32 can be written as follows:

$$\cot\left(k\frac{l}{2}\right) = -\frac{1}{\pi k r_0^2}\frac{r^2}{r+2t/\pi}. \tag{3}$$

Here l is the tube length, r_0 is its inner diameter, t is the wall thickness, and r is the hole diameter, assuming it is circular. We can approximate the slit by a round hole of the same area; this yields $r=0.155$ mm. $k=2\pi f/c$, where f is the frequency and c is the speed of sound, which we shall assume to be 345 m/s. Using Eq. (3), l can be explicitly expressed as a function of k or f. Subsequently, we used an inverse function to plot the experimental results against $f(l)$. Figure 3 shows the square of the QEPAS signal normalized to the H_2O concentration. The points were fitted with a Lorentzian profile, which describes power in the classical driven oscillator as a function of frequency. The fitting curve is centered at $f_{res}=32.11$ kHz and has a FWHM=5.78 kHz, corresponding to $Q=5.6$, similar to values reported by Serebryakov *et al.* in Ref. 31. The tube length corresponding to f_{res} is $l_{res}=7.74$ mm. This is very close to $l_{f0}=7.56$ mm from Eq. (3) for the actually measured QTF resonant frequency $f_0=32\,750$ Hz.

The mR used in the studies described below was 8 ± 0.1 mm long, while the other geometrical parameters remained the same. According to the fitting curve in Fig. 3, this

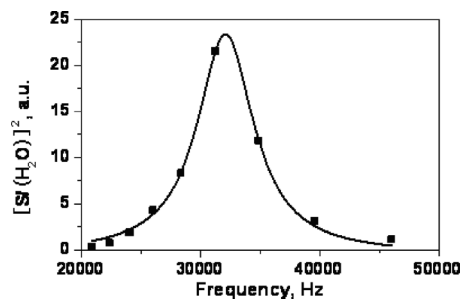

FIG. 3. Square of the OB-QEPAS signal as a function of $f(l)$, which is the resonant frequency calculated for each microresonator length using Eq. (3). The experimental results are fitted with a Lorentzian curve.

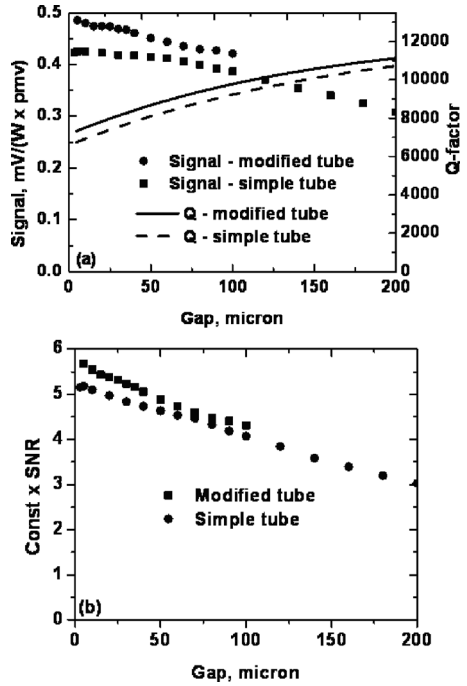

FIG. 4. (a) OB-QEPAS signal and Q-factor of the QTF as a function of the distance between the mR and the QTF. (b) Relative SNR as a function of the gap between QTF and outer mR surface.

results in a 10% lower signal compared to the optimum length. For this geometry it was determined that the maximum signal is obtained when the mR is centered 0.8 mm below the QTF tips. So, in the measurements described further in this paper, the mR was positioned in this manner. The optimum resonator position appeared to be similar to the optimum laser beam position in the on-beam, no mR QEPAS detection scheme (0.7 mm below the QTF tips).[17,29]

For OB-QEPAS, the distance between the mR and the QTF is also critical for optimum spectrophone performance. Too long a distance will decrease the acoustic coupling between mR and QTF, while too short a distance may dampen the QTF vibration because of the viscous drag. Figure 4(a) shows the OB-QEPAS signal of H_2O as a function of the distance between the mR and the QTF for two microresonators: a simple tube as shown in Fig. 2(a), and a modified tube shown in Fig. 2(b). Smooth curves approximating the experimentally measured Q-factor are also shown in the same plot. The Q-factor was measured by means of the control electronics unit described in Ref. 19, along with the QTF resonant frequency f_0 and its dynamic resistance R. It is known that the fundamental thermal noise of QTF is proportional to $\sqrt{Q}$. Figure 4(b) shows the relative SNR calculated as the signal from Fig. 4(a) divided by $\sqrt{Q}$ and multiplied by a constant number for convenience of presentation. We do not need the absolute SNR here (H_2O concentration dependent) to compare performance of the spectrophones and therefore use this easier-to-calculate value. Close proximity of the QTF to mR results in a better acoustic coupling, and therefore a higher signal and SNR. At the same time, viscous drag in the air layer between the QTF and mR reduces the Q-factor. Regardless of this unwanted effect, the SNR exhibits close-to-linear growth down to a 5 μm gap. A modified mR provides

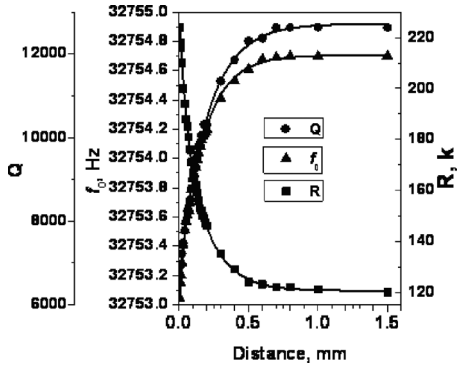

FIG. 5. QTF parameters as function of the distance between the mR and the QTF. Q is the quality factor of the QTF; f_0 is QTF resonant frequency; and R is the equivalent resistance of the QTF.

a ~10% better SNR, because of the reduced viscous drag thanks to enlarged space between the QTF and the tube surfaces.

Figure 5 shows the QTF parameters measured for a wider range of the QTF-mR separation distance. These data can be used to compare theoretical and numerical modeling of this spectrophone configuration with experimental results.

The dependence of the Q factor and the resonant frequency of the QTF on the distance between the mR and the QTF can be closely approximated by the exponential function

$$y = y_0 + A_1(1 - e^{-ax}), \tag{4}$$

where x is the distance between the mR and the QTF. Fitting parameters obtained for Q-factor of the QTF used in present work and a simple tube mR are as follows: $y_0 = 6599 \pm 37$, $A_1 = 6119 \pm 46$, and $a = 5.0 \pm 0.1$ mm^{-1}, and for the resonant frequency f are: $y_0 = 32753.08 \pm 0.02$ Hz, $A_1 = 1.61 \pm 0.02$ Hz, and $a = 6.4 \pm 0.2$ mm^{-1}. The same fitting parameters obtained for the Q factor of the modified mR tube are: $y_0 = 7167 \pm 40$, $A_1 = 5500 \pm 45$, and $a = 5.7 \pm 0.1$ mm^{-1}, and for the resonant frequency f are: $y_0 = 32753.18 \pm 0.01$ Hz, $A_1 = 1.271 \pm 0.013$ Hz, and $a = 7.1 \pm 0.2$ mm^{-1}.

IV. SENSOR PERFORMANCE EVALUATION

When the gas pressure changes, it affects many aspects of the QEPAS based sensing such as the absorption line intensity, V-T relaxation rate of the initially excited state, Q-factors of both the mR and the QTF, and acoustic coupling between the QTF and the mR. Therefore, we investigated the sensor performance at different pressures.

Figure 6 shows the normalized OB-QEPAS signal at the peak of the absorption line as a function of modulation amplitude at different pressures. Figure 7(a) depicts the maximum signal as a function of pressure and the corresponding parameters of the QTF. As mentioned earlier, the ratio of the signal to $\sqrt{Q}$ is proportional to SNR, and it is shown in Fig. 7(b). While the maximum signal for H_2O detection was obtained at a pressure of 120 Torr (2.2 times higher than at 760 Torr), the best SNR was achieved at 155 Torr.

If the observed signal is normalized to the Q-factor of the QTF, it provides a measure of the acoustic pressure acting on the QTF. These data are presented in Fig. 7(c). The solid curve shows a numerically simulated optimum $2f$ absorption signal (effective absorption coefficient, as in Ref. 29) as a function of pressure. It can be seen that the experimentally observed acoustic pressure acting upon the QTF closely follows. This result is somewhat surprising. Indeed,

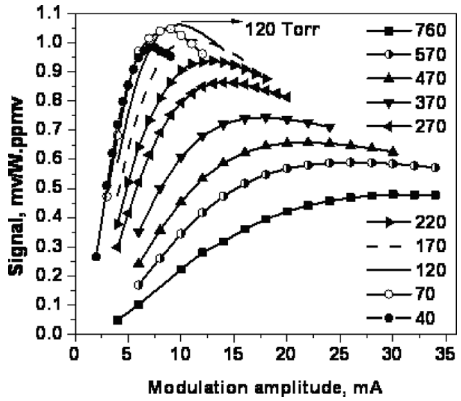

FIG. 6. Normalized OB-QEPAS signal measured for H_2O vapor at the peak of 7161.41 cm^{-1} absorption line as a function of modulation amplitude. Mean laser current is 68 mA. Total gas pressure in torr is indicated for each curve in the legend.

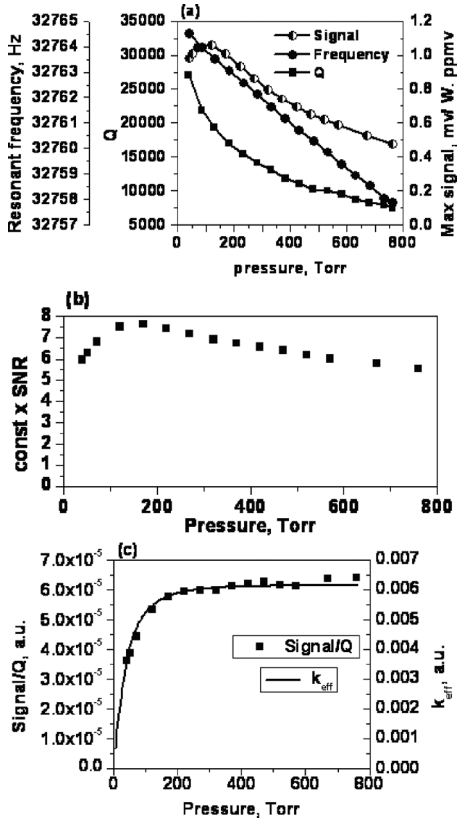

FIG. 7. (a) Normalized maximum OB-QEPAS signal measured for H_2O vapor and QTF parameters as a function of pressure. Signal, normalized maximum OB-QEPAS signal of H_2O vapor; frequency, resonant frequency of the QTF; Q is the quality factor of the QTF. (b) Signal to noise ratio multiplied by a constant. (c) OB-QEPAS signal normalized to the Q-factor of the QTF. Solid curve is a numerically simulated effective absorption coefficient k_{eff} described in Ref. 29. It represents the peak value of $2f$ wavelength modulation signal in absorption spectroscopy when the modulation sweep is optimal.

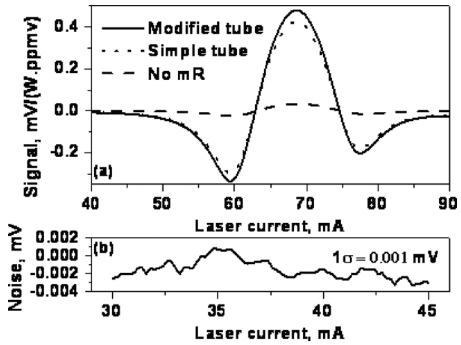

FIG. 8. (a) Normalized H_2O absorption spectrum acquired by different QEPAS schemes. "Simple, modified"-OB-QEPAS signal acquired with the simple and modified mR tubes; "no mR"-QEPAS signal acquired using QTF without microresonator. (b) Background noise measurement for OB-QEPAS with a modified mR tube. All of the measurements are carried out at normal atmospheric pressure.

the acoustic pressure must be proportional to the product of k_{eff} and the mR Q-factor, which in turn is expected to be proportional to $P^{1/2}$, where P is the gas pressure. This discrepancy will be a subject of further investigation.

For comparison, QEPAS signals of H_2O in air measured at normal atmospheric pressure without a microresonator, and OB-QEPAS H_2O signals using a mR with both simple and modified tubes are shown in Fig. 8(a). The distance between the mR and the QTF was fixed at ~ 10 μm for the OB-QEPAS measurements. The QTF signals depicted in Fig. 8(a) are normalized to the H_2O concentration, as the atmospheric H_2O vapor concentration was not constant during the measurements. The H_2O concentration was determined by using direct absorption spectroscopy with a 33 cm long optical gas cell. From these measurements we can deduce that the signals obtained with OB-QEPAS using a simple tube and modified tube mRs were 12.8 and 14.4 times greater, respectively, than that of a QEPAS sensor with only a QTF.

It was previously verified that the fundamental limitation of the QEPAS sensitivity was determined by the thermal excitation of the QTF.[17,23,30] The theoretical thermal noise level of the QTF at its resonant frequency can be calculated from the following expression:[33]

$$\sqrt{\langle V_N^2 \rangle} = \sqrt{\Delta f} R_g \sqrt{\frac{4k_B T}{R}}, \tag{5}$$

where $\sqrt{\langle V_N^2 \rangle}$ is the rms voltage noise at the transimpedance amplifier output, Δf is the detection bandwidth, k_B is the Boltzmann constant, R_g is the gain resistor of the transimpedance amplifier, T is the temperature, and R is the electrical parameter of the QTF when it is represented by the equivalent serial resonant. For the optimized OB-QEPAS gas sensor reported in this article, R_g was 10 MΩ, the value of the R was measured to be 203 kΩ, and Δf was 0.094 Hz. If we assume a temperature of 300 K, with a 0.094 Hz detection bandwidth, the calculated theoretical noise level of the OB-QEPAS based sensor was 0.875 μV.

For determining the noise level of the optimized OB-QEPAS based gas sensor, the laser wavelength was thermally tuned to a spectral region free from H_2O absorption. This allowed a determination of the noise level using the standard deviation value deduced from baseline measurements, shown in Fig. 8(b). A 1σ noise level of 1 μV was deduced for a 1 s integration time with an 18 dB/octave slope filter (0.094 Hz detection bandwidth). This noise level was in good agreement with the theoretical prediction taking into account the measurement uncertainties. The optimized OB-QEPAS signal at the 7161.41 cm^{-1} absorption line center of H_2O at 1.46% concentration was measured to be 56.03 mV at normal atmospheric pressure. Therefore, the SNR was 56 000, which corresponds to a minimum detectible concentration of 0.26 ppmv for H_2O when using a laser power of ~ 8 mW. For H_2O detection at normal atmospheric pressure a normalized noise equivalent absorption coefficient, $\text{NNEA}(1\sigma) = 6.2 \times 10^{-9}$ cm^{-1} $W/Hz^{1/2}$ was obtained.

Knowing that the detector noise is described by Eq. (5) and hence is proportional to $\sqrt{Q}$, and using the quality factor data from Figs. 4(a) and 5, we can calculate a SNR gain (SNRG) obtained in OB-QEPAS as $\text{SNRG} = 12.8\sqrt{12\,700/6900} = 17.3$ for a simple tube, and $\text{SNRG} = 14.4\sqrt{12\,700/7500} = 18.7$ for a modified tube.

V. CONCLUSIONS

A drop in the QTF quality factor when the QTF is incorporated into the OB-QEPAS spectrophone is small (from 13 000 to 8000), indicating a relatively weak mR to QTF coupling compared to the on-beam configuration, where the Q changes from 13 000 to as low as 1380.[34] This weaker coupling is partially compensated by lower losses in the mR tube. Comparing the SNRG of OB-QEPAS to the on-beam spectrophone design, we found that the optimum on-beam design has a $\sim 1.6-1.7$ better SNR at atmospheric pressure. However, OB-QEPAS is more flexible regarding the QTF geometry. For example, QTFs with a smaller gap between the prongs can be used without a possible obstruction of the excitation radiation. The OB-QEPAS spectrophone may also be technologically easier to assemble and align.

ACKNOWLEDGMENTS

This research was funded by the National 863 High Technology Research and Development Program of China under Grant No. 2006AA06Z237, and in part by the French International Research Program CNRS/SAMIA. The Rice Laser Science Group acknowledges partial funding from a National Science Foundation Engineering Research Center MIRTHE grant, from the Welch Foundation (Grant No. C-0586) and an award from the Rice University President's International Travel Fund.

[1] G. Wysocki, Y. Bakhirkin, S. So, F. K. Tittel, C. J. Hill, R. Q. Yang, and M. P. Fraser, Appl. Opt. **46**, 8202 (2007).
[2] S. M. Cristescu, S. T. Persijn, S. T. Hekkert, and F. J. M. Harren, Appl. Phys. B: Lasers Opt. **92**, 343 (2008).
[3] M. R. McCurdy, Y. Bakhirkin, G. Wysocki, R. Lewicki, and F. K. Tittel, J. Breath Res. **1**, 014001 (2007).
[4] I. Linnerud, P. Kaspersen, and T. Jager, Appl. Phys. B: Lasers Opt. **67**, 297 (1998).
[5] F. G. C. Bijnen, J. Reuss, and F. J. M. Harren, Rev. Sci. Instrum. **67**, 2914 (1996).
[6] A. Miklós, P. Hess, and Z. Bozóki, Rev. Sci. Instrum. **72**, 1937 (2001).
[7] A. Schmohl, A. Miklós, and P. Hess, Appl. Opt. **41**, 1815 (2002).
[8] M. G. da Silva, H. Vargas, A. Miklos, and P. Hess, Appl. Phys. B: Lasers

Opt. **78**, 677 (2004).
[9] S. Schilt, L. Thevenaz, M. Nikles, L. Emmenegger, and C. Huglin, Spectrochim. Acta, Part A **60**, 3259 (2004).
[10] J. S. Li, X. M. Gao, L. Fang, W. J. Zhang, and H. Cha, Opt. Laser Technol. **39**, 1144 (2007).
[11] L. B. Kreuzer, J. Appl. Phys. **42**, 2934 (1971).
[12] M. E. Webber, M. Pushkarsky, and C. K. N. Patel, Appl. Opt. **42**, 2119 (2003).
[13] F. J. M. Harren, J. Reuss, E. J. Woltering, and D. D. Bicanic, Appl. Spectrosc. **44**, 1360 (1990).
[14] P. L. Meyer and M. W. Sigrist, Rev. Sci. Instrum. **61**, 1779 (1990).
[15] J. S. Li, X. M. Gao, W. Z. Li, Z. S. Cao, L. H. Deng, W. X. Zhao, M. Q. Huang, and W. J. Zhang, Spectrochim. Acta, Part A **64**, 338 (2006).
[16] V. Koskinen J. Fonsen1, K. Roth, and J. Kauppinen, Appl. Phys. B: Lasers Opt. **86**, 451 (2007).
[17] A. A. Kosterev, Y. A. Bakhirkin, R. F. Curl, and F. K. Tittel, Opt. Lett. **27**, 1902 (2002).
[18] A. A. Kosterev and F. K. Tittel, Appl. Opt. **43**, 6213 (2004).
[19] R. Lewicki, G. Wysocki, A. A. Kosterev, and F. K. Tittel, Appl. Phys. B: Lasers Opt. **87**, 157 (2007).
[20] A. A. Kosterev, T. S. Mosely, and F. K. Tittel, Appl. Phys. B: Lasers Opt. **85**, 295 (2006).
[21] S. Schilt, A. A. Kosterev, and F. K. Tittel, Appl. Phys. B: Lasers Opt. **95**, 813 (2009).
[22] A. A. Kosterev, Y. A. Bakhirkin, F. K. Tittel, S. Mcwhorter, and B. Ashcraft, Appl. Phys. B: Lasers Opt. **92**, 103 (2008).
[23] K. Liu, J. Li, L. Wang, T. Tan, W. Zhang, X. Gao, W. Chen, and F. K. Tittel, Appl. Phys. B: Lasers Opt. **94**, 527 (2009).
[24] M. Horstjann, Y. A. Bakhirkin, A. A. Kosterev, R. F. Curl, F. K. Tittel, C. M. Wong, C. J. Hill, and R. Q. Yang, Appl. Phys. B: Lasers Opt. **79**, 799 (2004).
[25] M. D. Wojcik, M. C. Phillips, B. D. Cannon, and M. S. Taubman, Appl. Phys. B: Lasers Opt. **85**, 307 (2006).
[26] M. C. Phillips, T. L. Myers, M. D. Wojcik, and B. D. Cannon, Opt. Lett. **32**, 1177 (2007).
[27] R. Lewicki, G. Wysocki, A. A. Kosterev, and F. K. Tittel, Opt. Express **15**, 7357 (2007).
[28] A. K. Y. Ngai, S. T. Persijn, I. D. Lindsay, A. A. Kosterev, P. Groß, C. J. Lee, S. M. Cristescu, F. K. Tittel, K.-J. Boller, and F. J. M. Harren, Appl. Phys. B: Lasers Opt. **89**, 123 (2007).
[29] N. Petra, J. Zweck, A. A. Kosterev, S. E. Minkoff, and D. Thomazy, Appl. Phys. B: Lasers Opt. **94**, 673 (2009).
[30] K. Liu, X. Guo, H. Yi, W. Chen, W. Zhang, and X. Gao, Opt. Lett. **34**, 1594 (2009).
[31] D. V. Serebryakov, I. V. Morozov, A. A. Kosterev, and V. S. Letokhov, Quantum Electron. **40**, 167 (2010).
[32] A. B. Pippard, *The Physics of Vibration* (Cambridge University Press, Cambridge, England, 1978), Vol. 1, Chap. 7.
[33] A. A. Kosterev, F. K. Tittel, D. V. Serebryakov, A. L. Malinovsky, and I. V. Morozov, Rev. Sci. Instrum. **76**, 043105 (2005).
[34] A. A. Kosterev, P. R. Buerki, L. Dong, M. Reed, T. Day, and F. K. Tittel, Appl. Phys. B **100**, 173 (2010).